A DEMONSTRATION OF PITCH-PLUNGE FLUTTER SUPPRESSION USING LQG CONTROL

A.N. Sutherland
Council for Scientific and Industrial Research
Aeronautic Systems Competency
P.O. Box 395, Pretoria, 0001, South Africa
Email: asutherland@csir.co.za, Tel.: +27 12 841 3880

Keywords: *Binary Flutter, Flutter Suppression, LQG Control*

Abstract

A new model wing incorporating a fullspan trailing edge control surface was designed and built to demonstrate active flutter suppression in low speed wind tunnels, using an existing small-scale pitch-plunge flexure mount. Open-loop flutter test results agreed well with predictions from classical flutter theory, and gentle low speed flutter was demonstrated. Closed-loop simulations using LQG control to drive the trailing edge control surface indicated that flutter can be suppressed successfully, despite the small size of the model. Physical implementation of the controller and its use in the wind tunnel flutter tests proved this to be so. The LQG flutter controller used to actuate the control surface was able to suppress flutter at speeds significantly higher than the open-loop flutter speed of the model, even when designed for that speed. Flutter suppression was demonstrated up to a speed 54m/s – an increase of 134% over the open-loop flutter speed of the model, at which point tests were arbitrarily stopped. This paper briefly describes the model and LQG controller, then presents and discusses some typical test results.

Nomenclature

ab	Distance between mid-chord and elastic axis
$\mathbf{A}$, $\mathbf{B}$, $\mathbf{C}$, $\mathbf{D}$	State-space matrices
b	Airfoil half-chord
c	Non-dimensional distance between airfoil mid-chord and control surface hinge line
C	Structural damping
$C(k)$	Theodorsen's function
δ, λ	Coefficients in rational approximation of Wagner function
$\mathbf{I}$	Identity matrix
k	Reduced frequency (Strouhal number)
K	Structural stiffness
ℓ_1, ℓ_2	1st and 2nd Aerodynamic lag state
L	Unsteady lift force
$\boldsymbol{\mathcal{L}}_\delta$, $\boldsymbol{\mathcal{L}}_\lambda$	Matrices of Wagner approximation function coefficients
m	Wing mass
M	Unsteady aerodynamic moment
Φ	Wagner function
$\mathbf{Q}_1$, $\mathbf{Q}_2$	Matrices of terms proportional to circulation about the aerofoil
ρ	Air density
T	Control surface position function
u	Control input
U	Free stream velocity
ω	Flutter frequency in *rad/s*
x_α	Non-dimensional distance between aerofoil pitch axis and aerofoil CG
x_β	Non-dimensional distance between control surface hinge axis and CG

Subscripts:

a	Aerodynamic
α	Pitch
β	Control surface angle
c	Command
h	Plunge
s	Structural

1. Introduction

Flutter is an important consideration in the design and performance of aircraft. Typically, aircraft are limited to a maximum speed that they should not exceed to ensure that flutter (which may result in the destruction of the airframe) is not encountered. Imposing a speed restriction on an aircraft is often undesirable, whilst ensuring the structure is sufficiently stiff to ensure that flutter won't be encountered in the operating airspeed range of the aircraft introduces a weight penalty that also acts to reduce the flight envelope of the aircraft and further limit its performance. An effective means of ensuring that flutter is not encountered during flight, without restricting the flight envelope of an aircraft, is to use primary aircraft control surfaces to actively damp out divergent oscillations characteristic of flutter.

It was shown in [1] that binary (pitch-plunge) flutter models are effective in demonstrating the concept of active flutter suppression as they exhibit gentle, low-speed, well defined flutter. The implementation of active flutter control is thus relatively easy, so these models also provide a means of evaluating the effectiveness of various control laws that could be extended and applied to a full scale aircraft. A novel active control binary flutter wind tunnel model design, as well as its mathematical representation and an active flutter suppression LQG controller design was detailed in [1].

This paper presents and describes results obtained with the model of [1] from tests conducted in the calibration (CWT) and low speed (LSWT) wind tunnels at the Council for Scientific and Industrial Research (CSIR).

2. Mathematical Model and Controller Design

Although given in detail in [1], a brief overview of the development of a mathematical model of the binary flutter system, as well as the state-space formulation of the model and control system design is given in this section for completeness.

2.1. Aeroelastic Model

Initially, the structural equations of motion of the binary flutter model need to be developed to be solved simultaneously with equations describing the aerodynamic forces acting on the model. To do this, Lagrange's equation (adapted to include Rayleigh's dissipation function) was applied to the flutter model depicted in Figure 2.1 and Figure 2.2, below.

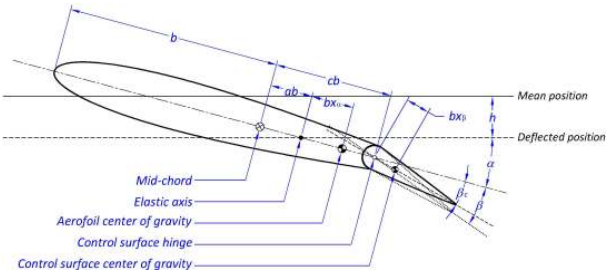

Figure 2.1 Pitch-Plunge Flutter Aerofoil Notation (Derived from [2])

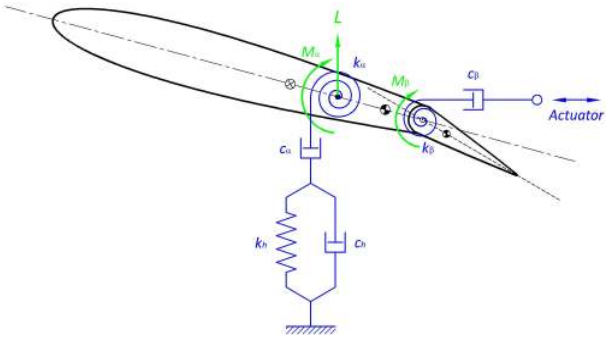

Figure 2.2 Fluttering Aerofoil Free Body Diagram (Derived from [2])

Using Lagrange's method, it can be shown that the linearised equations of motion of the system are [3]:

$$m\ddot{h} + mx_\alpha b\ddot{\alpha} + mx_\beta b\ddot{\beta} + C_h h + K_h h = L \quad \text{.....(2.1)}$$

$$mx_\alpha b\ddot{h} + I_\alpha \ddot{\alpha} + \left[(c-a)b^2 mx_\beta + I_\beta\right]\ddot{\beta} + C_\alpha \dot{\alpha} + K_\alpha \alpha = M_\alpha \quad \text{.....(2.2)}$$

$$mx_\beta b\ddot{h} + \left[(c-a)b^2 mx_\beta + I_\beta\right]\ddot{\alpha} + I_\beta \ddot{\beta} + C_\beta \dot{\beta} + K_\beta(\beta - \beta_c) = M_\beta \quad \text{...(2.3)}$$

where the forces acting on the aerofoil are the unsteady lift 'L' (assumed to act at the quarter chord position), unsteady pitching moment 'M_α' and unsteady control surface hinge moment 'M_β'. Theodorsen's method [4] was used to model these forces. This method is limited to aerofoils with thin sections of infinite span undergoing small oscillations in all vibration

modes. Flow over the aerofoil is assumed to remain potential and un-separated. In view of this, the unsteady lift, pitching moment and control surface hinge moment are described in terms of the instantaneous configuration of the system (position, rate and acceleration of all vibration modes) per unit wingspan and are then given as [4]:

$$L = -\rho b^2\left(\pi\ddot{h} - \pi ba\ddot{\alpha} - bT_1\ddot{\beta} + U\pi\dot{\alpha} - UT_4\dot{\beta}\right) - 2\pi\rho bC(k)\left[\dot{h} + b\left(\tfrac{1}{2}-a\right)\dot{\alpha} + \tfrac{1}{2\pi}bT_{11}\dot{\beta} + U\alpha + \tfrac{1}{\pi}T_{10}U\beta\right] \quad \text{.....(2.4)}$$

$$M_\alpha = -\rho b^2\left\{-\pi ab\ddot{h} + \pi b^2\left(\tfrac{1}{8}+a^2\right)\ddot{\alpha} - b^2\left[T_7 + (c-a)T_1\right]\ddot{\beta} + \pi bU\left(\tfrac{1}{2}-a\right)\dot{\alpha} + bU\left[T_1 - T_8 - (c-a)T_4 + \tfrac{1}{2}T_{11}\right]\dot{\beta} + (T_4+T_{10})U^2\beta\right\} - 2\pi\rho b^2U\left(\tfrac{1}{2}+a\right)C(k)\left[\dot{h} + b\left(\tfrac{1}{2}-a\right)\dot{\alpha} + \tfrac{1}{2\pi}bT_{11}\dot{\beta} + U\alpha + \tfrac{1}{\pi}T_{10}U\beta\right] \quad \text{.....(2.5)}$$

$$M_\beta = -\rho b^2\left\{-bT_1\ddot{h} + 2b^2T_{13}\ddot{\alpha} - \tfrac{1}{\pi}b^2T_3\ddot{\beta} - Ub\left[2T_9 + T_1 - T_4\left(\tfrac{1}{2}-a\right)\right]\dot{\alpha} - \tfrac{1}{2\pi}UbT_4T_{11}\dot{\beta} + \tfrac{1}{\pi}U^2\left(T_5 - T_4T_{10}\right)\beta\right\} - \rho b^2UT_{12}C(k)\left[\dot{h} + b\left(\tfrac{1}{2}-a\right)\dot{\alpha} + \tfrac{1}{2\pi}bT_{11}\dot{\beta} + U\alpha + \tfrac{1}{\pi}T_{10}U\beta\right] \quad \text{.....(2.6)}$$

where the 'T' terms are a function of the control surface position and can be found in [4]. *C(k)* accounts for lift due to vortices being shed off the trailing edge of the wing because of its motion, and is expressed in terms of Bessel (or Hankel) functions. To model these aerodynamic lag effects, a rational approximation to Theodorsen's function is needed. This is achieved by solving a two-term approximation of Wagner's function (which is the inverse Fourier transform of Theodorsen's function divided by $i\omega$, as shown in Equation (2.7)), given in Equation (2.8) [5]:

$$\Phi = \mathcal{F}^{-1}\left\{\frac{C(k)}{i\omega}\right\} \quad \text{.....(2.7)}$$

$$\Phi = 1 - \delta_1 e^{\frac{-\lambda_1 Ut}{b}} - \delta_2 e^{\frac{-\lambda_2 Ut}{b}} \quad \text{.....(2.8)}$$

In Equation (2.8) it is assumed that $\delta_1 = 0.165$, $\lambda_1 = 0.041$, $\delta_2 = 0.335$ and $\lambda_2 = 0.320$ as given in [5]. Equations (2.1), (2.2) and (2.3) (structural equations of the system) are combined with Equations (2.4), (2.5) and (2.6) (generalised aerodynamic forces) to form the equations of motion of the system. Equation (2.8) is used to approximate the circulatory lift contribution to the unsteady aerodynamic forces. The combined equations (not shown) are then written in a state-space form so that an appropriate control system can be designed, as described briefly in §2.2 and §2.3.

2.2. State-Space Model

Using time domain control theory, the state-space equations of motion of the dynamic system are [6]:

$$\left.\begin{aligned}\dot{\mathbf{X}} &= \mathbf{AX} + \mathbf{B}u\\ \mathbf{Y} &= \mathbf{CX}\end{aligned}\right\} \quad \text{.....(2.9)}$$

where $u = \beta_c$ is the commanded flap angle. The development of the system matrix **A**, the input matrix **B** and the measurement matrix **C** is beyond the scope of this paper, although they are listed in Appendix A for completeness. The system consists of eight states viz. the plunge deflection, pitch angle, control surface angle, their respective rates and two aerodynamic lag states (since a two-term approximation to the Wagner function is used). In vector notation that is:

$$\mathbf{X} = \left[\dot{h} \quad \dot{\alpha} \quad \dot{\beta} \quad h \quad \alpha \quad \beta \quad \ell_1 \quad \ell_2\right]^T \quad \text{.....(2.10)}$$

During wind tunnel testing, the plunge displacement, pitch angle and control surface angle were measured and the remaining five states were estimated using a Kalman filter. Further discussion of this and a brief overview of the control system design is given in §2.3.

2.3. Control System Design

A linear quadratic Gaussian (LQG) controller was designed to suppress flutter. This controller consisted of a linear quadratic regulator (LQR) controller to calculate feedback gains and a Kalman filter to estimate unmeasured system states. The controller was designed using the control system toolbox in MATLAB™. A complete block diagram model of the flutter system was also developed in Simulink™ to investigate the effect of nonlinearities in the system on the model's closed-loop response.

3. Wind Tunnel Model and Apparatus

The wind tunnel model designed to demonstrate the principle of active flutter suppression for this work was designated as the FAST (Flutter with Active Suppression Technology) wind tunnel model. It consists of a novel flexure mount [1] to provide the structural dynamics, a straight wing with a NACA0012 profile and trailing edge control surface, a linear actuator to drive the control surface, a USB data acquisition system and custom software to acquire data, estimate system states and apply feedback control to the model. A brief overview of each of these FAST model components is given in the subsections that follow.

3.1. Wind Tunnel Model

3.1.1. Pitch-Plunge Flutter Model Mount

The flexure mount system designed to provide the structural dynamics for the FAST model was based on Farmer's [7] design, but uses rectangular instead of round flexures. The use of rectangular flexures allows the central drag strut in the original design to be omitted and makes the small size of the FAST wind tunnel model feasible. The pitch and plunge frequencies of the model can be tailored by adjusting the angle of the rectangular flexures, thereby allowing the flutter dynamics of the model to be varied. The mount also incorporates ballast arms and sliding masses that can be used to alter the centre of gravity (CG) position and mass inertia of the model to enable various flutter cases to be set up.

3.1.2. Active Control Wing

The new FAST model wing comprised built-up carbon fibre and aluminium spars and ribs to which a load carrying carbon fibre skin sleeve attaches with brass M2 shoulder screws. This skin provides additional structural stiffness and the required aerodynamic shape. The control surface is a bonded structure of carbon fibre (intermediate ribs and skins) and aluminium (end and central ribs), and rotates in brass bushes located in the aluminium ribs. For these tests, the control surface was balanced so that its centre of mass coincided with its rotation axis. The wing parameters are given in Table 3.1 and the wing on the flexure mount is shown in Figure 3.1.

Table 3.1 FAST Model Wing Parameters

Wing Parameter	Value
Wingspan	360*mm*
Wing Chord	120*mm*
Wing Aspect Ratio	3
Wing Taper Ratio	1
Wing Twist	0.0*deg.*
Wing Aerofoil Section	NACA0012
Control Surface Span	346*mm*
Control Surface Chord	30*mm*

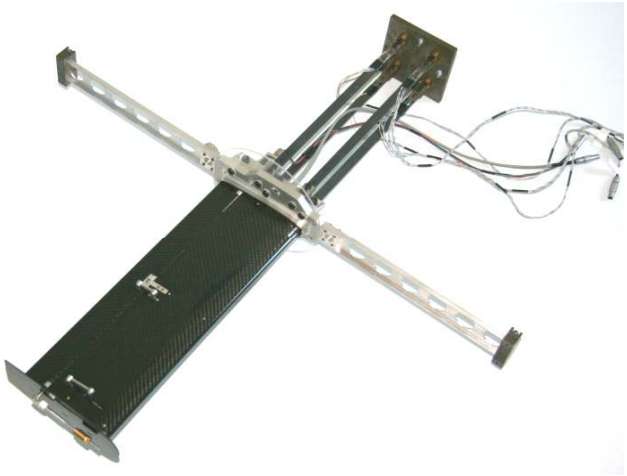

Figure 3.1 FAST Wind Tunnel Model

3.1.3. Control Surface Actuator and FAST Model Instrumentation

Initially it was decided that a model aircraft servo be used to actuate the control surface. These servos have been used in similar research (see for example [8]), but can suffer from free-play in the gears, dead-band, relatively high time constants which introduce significant time lag into the control system and at the small size needed for this model, insufficient capacity to cope with the fairly high control surface inertia. For these reasons it was decided to use a larger,

externally mounted actuator that was powerful and fast enough to suppress the estimated flutter conditions. This actuator also provides more scope for future control algorithm testing and is more capable of suppressing flutter significantly beyond the open-loop critical flutter speed of the model.

A Faulhaber™ 1247-020-01 linear DC-Servomotor was chosen because of its impressive performance in terms of load and acceleration. The actuator, its mounting bracket, and the drive linkage/crank used to change the control surface angle are shown in Figure 3.2.

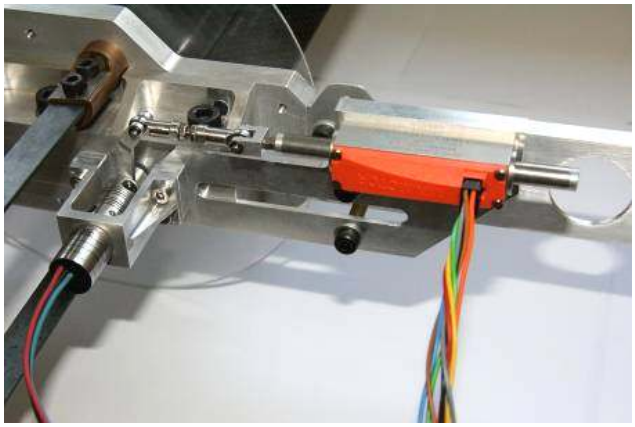

Figure 3.2 Control Surface Actuator, Actuation Mechanism and Angle Sensor

Two full strain gauge bridges (SGBs) at the root of the FAST model mount (Figure 3.3) are used to measure the pitch angle and plunge deflection of the wing as it oscillates. The pitch SGB was set up to measure differential bending in the flexures, not actual torsion of each of the flexures, so it gave zero output during pure bending of the mount. Thus the plunge SGB outputs its maximum signal and the pitch SGB outputs zero when the mount experiences pure translation and *vice versa* for pure rotation of the mount. Interference between the pitch and plunge bridges arising from slight misalignments and unaccounted for torsion in each flexures was calibrated out.

A Contelec™ Vert X-13 Hall effect rotary sensor with a measurement range of 0° to 360° and resolution of 0.01° was used to measure the control surface angle. This sensor was attached to the control surface shaft via a flexible coupling, as seen in Figure 3.2.

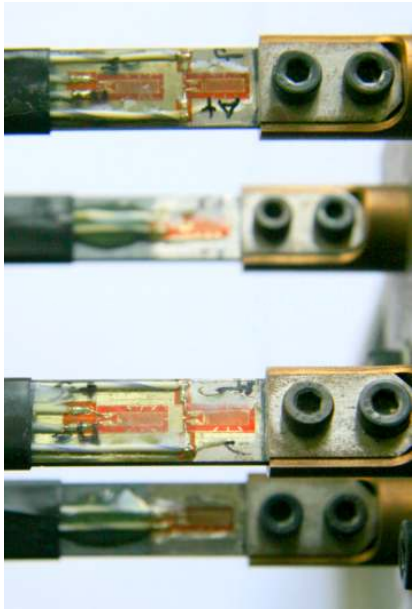

Figure 3.3 Pitch Angle and Plunge Deflection Strain Gauge Bridges

3.2. Data Acquisition and Control Software

The FAST model data acquisition (DAQ) and control software was written in Microsoft Visual™ C# (Express Edition), chosen because it is freely available, has built in database functionality, supports multi-threaded applications and is relatively easy to use. The design requirements of the software were to acquire data from the National Instruments™ NI USB-6211 data acquisition card, calculate Kalman state estimates, apply feedback gains and calculate control inputs, command the control surface actuator and log all data to file. Software threading was required to make these various components of the program run simultaneously at the relatively high frequencies required. An example screenshot of the main tab of this data acquisition and control application is shown in Figure 3.4.

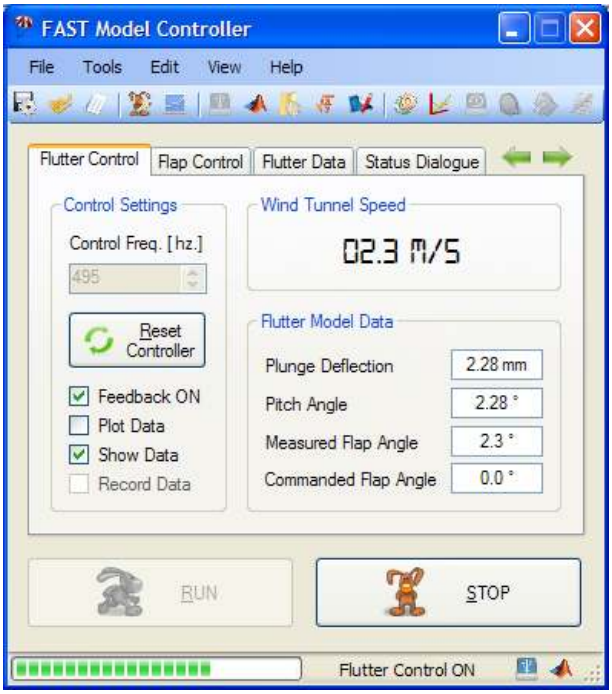

Figure 3.4 FAST Model Controller Software Interface

3.3. Wind Tunnels

Two wind tunnels at the CSIR were used to test the active flutter suppression model. Open-loop, and the majority of closed-loop wind tunnel testing of the FAST model was conducted in the CSIR's calibration wind tunnel (CWT), whilst limited closed-loop testing was conducted in the CSIR's low speed wind tunnel (LSWT). A brief description of each of these wind tunnels is given in §3.3.1 and §3.3.2.

3.3.1. Calibration Wind Tunnel

The CWT (shown in Figure 3.5) is a wooden blow-down tunnel with a $0.8m$ by $0.6m$ hexagonal test section. The CWT is ideal for flutter testing because of its small size, low turbulence and excellent velocity resolution. It has a speed range of 0.5 to $35.0m/s$ that can be adjusted by placing various gauzes behind the test section. For wind tunnel tests performed on the FAST wind tunnel model, only the open wind tunnel configuration was used. This was to allow the maximum wind tunnel speed to be achieved during closed-loop testing.

Figure 3.5 Calibration Wind Tunnel

3.3.2. Low Speed Wind Tunnel

The LSWT is a continuous wind tunnel with an adjustable atmospheric slot to vary the pressure within its $2.1m$ by $1.5m$ rectangular test section. It has a maximum operating speed of nominally $120.0m/s$. A schematic of the LSWT is shown in Figure 3.6, below.

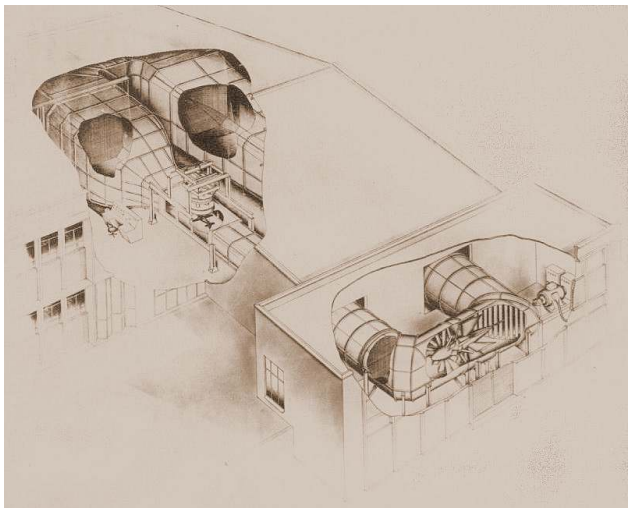

Figure 3.6 Low Speed Wind Tunnel

4. Results

The results from the set up and calibration, as well as wind tunnel testing of the FAST wind tunnel model are presented in this section. Prior to wind tunnel testing of the FAST model, the pitch and plunge SGBs and the control surface angle sensor were calibrated, and the transfer function of the control surface actuator and actuation mechanism was determined. These results are presented in §4.1 and §4.2,

respectively. The anticipated open-loop flutter speed of the FAST model was calculated and various closed-loop simulations performed for various model configurations before wind tunnel testing of the model commenced. Results from these calculations and simulations are briefly discussed in §4.3. Thereafter, selected results from open- and closed-loop wind tunnel testing of the FAST model in the CWT and LSWT are presented in §4.4.

4.1. Transducer Calibrations

The two SGBs at the root of the FAST model flexure mount were calibrated using a specifically designed calibration jig. The purpose of the jig was to fix the pitch degree of freedom of the mount whilst allowing motion in the plunge degree of freedom and *vice versa*. The model mount was calibrated with the static deflection of the wing-mount combination as the mean calibration point in both the plunge and pitch degrees of freedom. The two SGB's were calibrated by loading the model whilst holding the pitch angle fixed and measuring the response from each SGB to a pure plunge displacement and then fixing the plunge displacement whilst measuring their response to a change in the models pitch angle. Cross terms where also measured where, the model was allowed to pitch and plunge simultaneously. The plunge and pitch calibration surfaces are shown in Figure 4.1 and Figure 4.2, respectively.

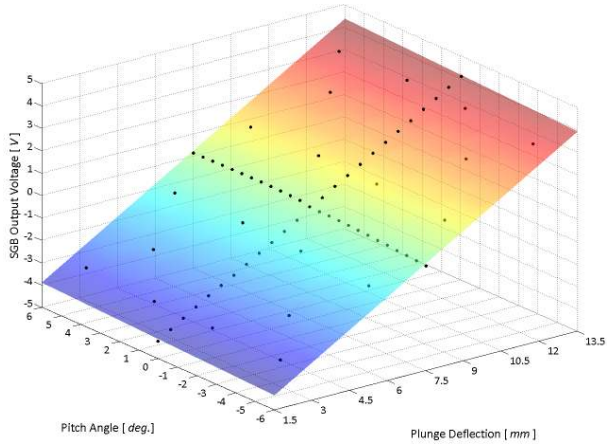

Figure 4.1 Plunge Strain Gauge Bridge Calibration Data and Fitted Surface

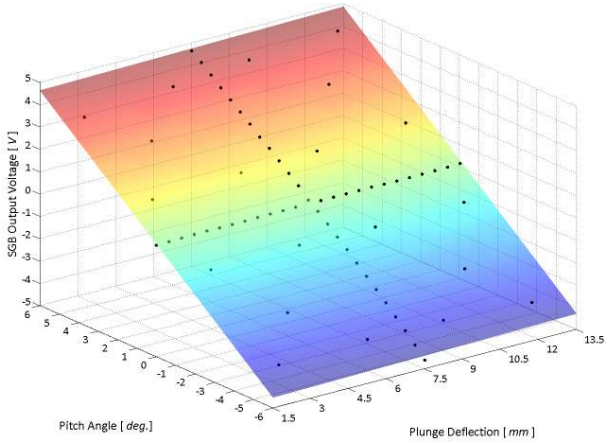

Figure 4.2 Pitch Strain Gauge Bridge Calibration Data and Fitted Surface

Plots of the residuals of each of these calibration surfaces showed that each fit was good and that both the pitch angle and plunge deflection strain gauge bridges are highly linear within the allowed deflection range of the mount.

4.2. Control Surface and Actuation Mechanism Transfer Function

The measured phase and normalised magnitude of the sub-system from a swept-sine input (from 1.0 to 12.0*Hz*.) using a *TTi* function generator (TG2000) was evaluated with a GenRad 2515 Computer-Aided Test System and plotted on a Bode diagram. A 2nd order Bessel filter was then fitted to the measured data to determine an approximate analytical transfer of the control surface and its actuation mechanism (see Figure 4.3). To validate the calculated analytical transfer function of the sub-system, the measured response of the control surface to a step input was compared to the step response predicted by the 2nd order Bessel filter. Figure 4.4 shows the good correlation obtained.

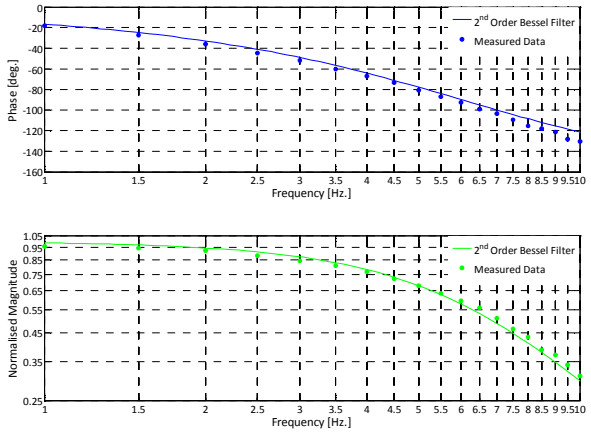

Figure 4.3 Control Surface and Actuation Mechanism Bode Diagram

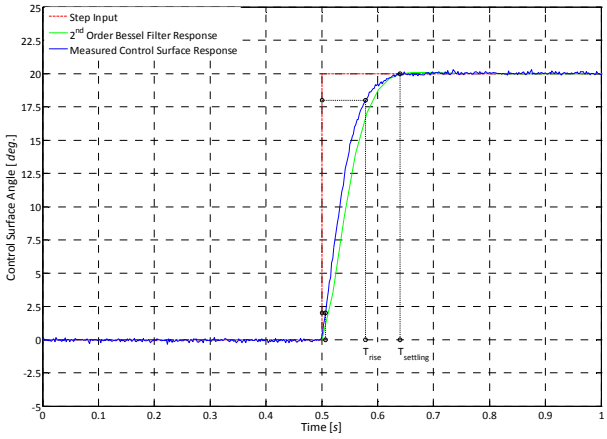

Figure 4.4 Control Surface and Actuation Mechanism Step Response

4.3. Open-Loop Flutter Predictions and Closed-Loop Simulations

The open-loop modal damping and frequencies of the FAST model were determined as a function of airspeed (see Figure 4.5) by solving the eigensolution of the state-space model of the system for various model configurations. This allowed the anticipated flutter speed of the model to be determined when evaluated at a case of zero damping.

Extensive simulations of the open- and closed-loop dynamics of the FAST model were done using models developed in both MATLAB™ and Simulink™ before wind tunnel tests were conducted. The purpose of these simulations was to establish the open-loop dynamics of the model and thereafter determine the anticipated effect and robustness of the implemented active flutter suppression controller. The advantage of the Simulink™ model was that the effect of nonlinearities (such as free-play, dead-band, time delays, etc.) that cannot be modelled easily in a sate-space system, could be investigated. The response of the model to an initial disturbance, impulse input and step input calculated from the MATLAB™ state-space model showed the control system to be robust at, and above the anticipated critical open-loop flutter speed of the model. The Simulink™ model showed that the controller was robust enough to not allow actual nonlinearities in the system to destabilise it and cause divergent oscillations of the model.

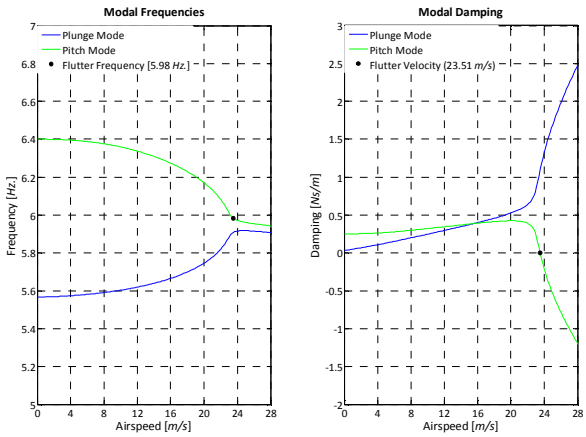

Figure 4.5 Open-Loop Damping and Frequency Response (Baseline CG Position)

4.4. Wind Tunnel Results

Three model configurations were tested in the CWT, whilst limited flutter boundary extension tests were performed in the LSWT. The FAST model configurations tested in the CWT were a baseline CG position configuration, a forward CG position configuration and an aft CG position configuration. Initially, open-loop wind tunnel testing was performed to observe the dynamics of the model and validate its state-space representation used in the controller design. Thereafter, closed-loop wind tunnel testing was performed for all three configurations up until the maximum operating speed of the CWT. Limited flutter boundary extension tests of the FAST model in its baseline CG position configuration were then performed in the LSWT because of its higher

operating speed. Selected results from open- and closed-loop tests performed in both the CWT and LSWT are given in §4.4.1 and §4.4.2, below.

4.4.1. Calibration Wind Tunnel Results

The open-loop flutter speed of the FAST model was carefully approached by analysing its sub-critical response at wind tunnel speeds well below its anticipated flutter speed. The power spectral densities (PSD's) were calculated from the sub-critical time response of the plunge displacement and pitch angle to determine the modal frequency and damping of the model. This data was then used to calculate the simplified Zimmerman flutter margin and predict an open-loop flutter speed for each FAST model configuration. A half-power bandwidth method was also used to analyse the sub-critical data and predict a flutter onset speed for the wind tunnel model in each of CG position configurations tested.

Once the critical flutter speed was safely approached, the model was allowed to flutter (as shown for example in Figure 4.6) so that data could be recorded to validate the mathematical model of the system used in the flutter suppression controller design.

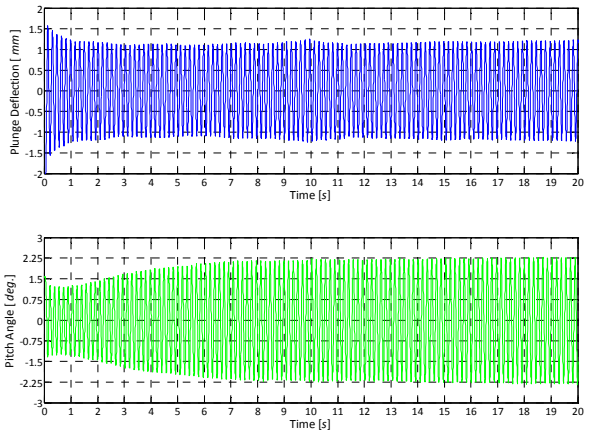

Figure 4.6 Open-Loop Flutter (Baseline CG Position; $U_f = 24.28 m/s$)

A plot of the normalised PSDs as a function of airspeed from the pitch angle SGB is shown in Figure 4.7 to illustrate how the two modal frequencies of the model converged on its flutter speed as the wind tunnel speed increased.

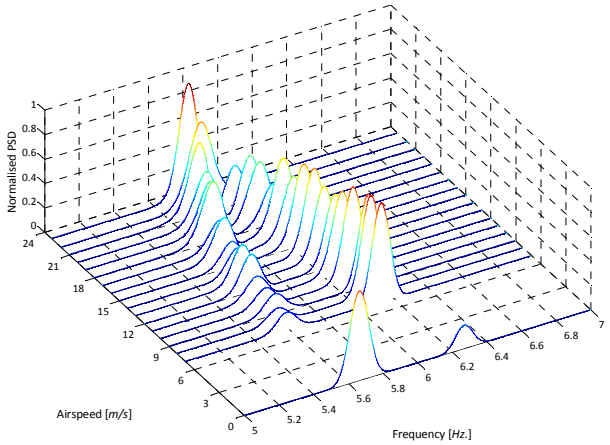

Figure 4.7 Combined Normalised Open-Loop PSDs (Pitch SGB, Baseline CG Position)

The calculated and measured flutter speeds and flutter frequencies of the FAST model in each CG position configuration tested are tabulated in Table 4.1 and Table 4.2, respectively.

Table 4.1 FAST Model Open-Loop Flutter Speeds

FAST Model Configuration (CG Position)	Flutter Speed		
	m/s		
	P-k Solution	Eigen Solution	Actual Value
Baseline	21.70	23.51	23.01
Forward	19.58	20.18	21.40
Aft	27.87	29.75	30.00

Table 4.2 FAST Model Open-Loop Flutter Frequencies

FAST Model Configuration (CG Position)	Flutter Frequency		
	Hz.		
	P-k Solution	Eigen Solution	Actual Value
Baseline	5.98	5.98	5.83
Forward	6.15	6.06	6.13
Aft	6.32	6.12	6.02

Closed-loop wind tunnel testing of the FAST model in the CWT was conducted once open-loop testing had been completed and the mathematical model of the system had been validated. During initial closed-loop wind tunnel tests, the control algorithm was activated and the wind tunnel speed set to the open-loop flutter speed with the FAST model held fixed. The model was then released to determine if the control law would prevent it from fluttering.

Having shown the FAST model would not flutter at (or slightly above) its open-loop critical flutter speed at each CG position configuration, the control law was deactivated and the model allowed to flutter for a short period of time. Once the model had established a flutter cycle the control system was re-activated to demonstrate its effectiveness in suppressing flutter. Figure 4.8 shows the response of the model near its critical open-loop flutter speed before and after the active flutter suppression feedback controller was activated.

The sub-critical response on the FAST model in its baseline CG position configuration with the control algorithm activated was also evaluated. The model was given an initial displacement and then allowed to oscillate freely at increasing wind tunnel speeds. The combined PSDs of the time series data obtained from these tests (see Figure 4.9) show the effectiveness of the control in separating the two modal frequencies of the model as well as adding damping to the system.

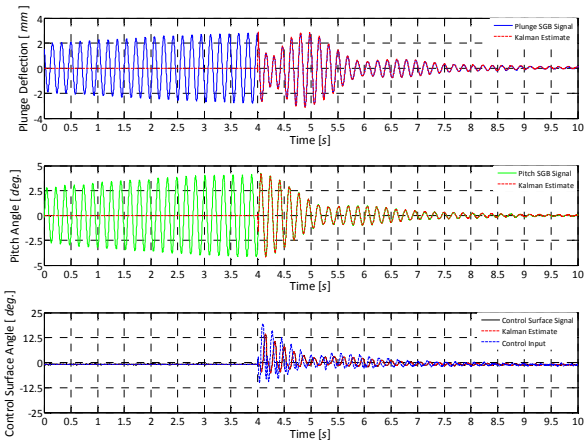

Figure 4.8 Closed-Loop Response (Baseline CG Position; $U = 24.52 m/s$)

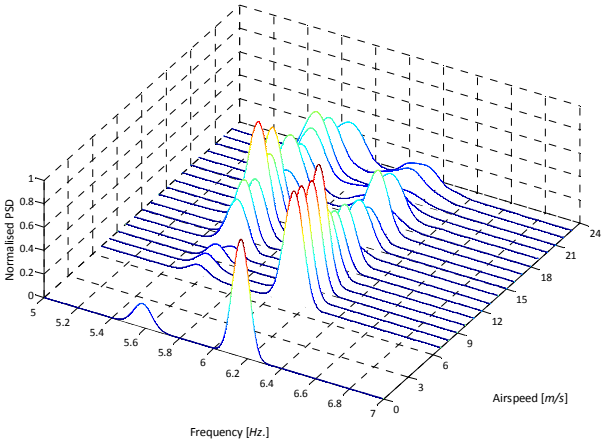

Figure 4.9 Combined Normalised Closed-Loop PSD's (Pitch SGB, Baseline CG Position)

Having demonstrated the effectiveness of the feedback controller designed in suppressing flutter, flutter boundary extension tests were conducted in the CWT. It was shown that the model could still be stabilised at the maximum operating speed ($35.60 m/s$) of the CWT with a controller designed for the critical open-loop flutter speed of the model in each CG position configuration.

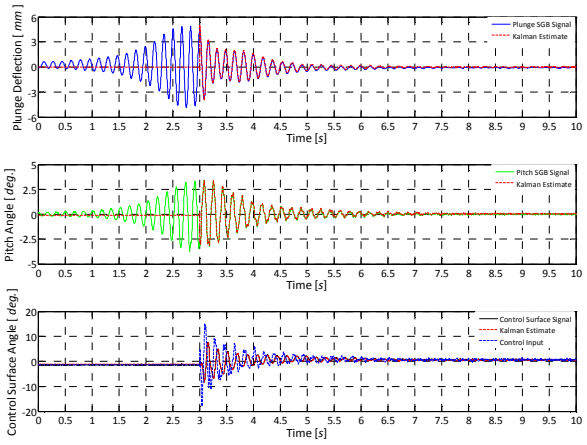

Figure 4.10 Closed-Loop Response (Baseline CG Position; $U = 35.60 m/s$)

4.4.2. Low Speed Wind Tunnel Results

Based on the excellent closed-loop response of the FAST model in the CWT, it was decided that the closed-loop control effectiveness of the baseline CG position configuration and the extent to which the flutter boundary of the FAST model could be extended, be tested in the LSWT. The LSWT was chosen because of its

higher operating speed (maximum nominally 120.0*m/s*). The FAST model was tested up to 53.91*m/s* in the LSWT. Testing beyond this point was deemed unsafe although the control law was still very effective at suppressing flutter at this speed. The damped closed-loop response of the model, after it was given an initial displacement at this wind tunnel speed of 53.91*m/s*, is shown in Figure 4.11.

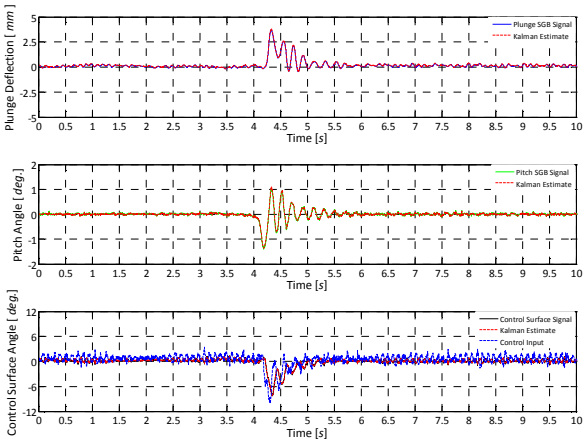

Figure 4.11 Closed-Loop Response (Baseline CG Position; $U = 53.91m/s$)

5. Discussion

Overall, the results obtained from open- and closed-loop testing of the FAST model in both the CWT and LSWT at the CSIR were very successful.

All transducers used to measure system states were carefully calibrated and a plot of the residuals showed them to be linear within their operating ranges. The transfer function (2^{nd} order Bessel filter) fitted to the measured response of the control surface actuator and actuation mechanism matched the measured response of this sub-system well. The step response of the control surface and its actuation mechanism showed that there was no lag, or any overshoot in this system. It was also determined from Figure 4.4 that the system has a rise time of 72*ms* and a settling time of 133*ms*.

Open-loop simulations of the FAST model performed in MATLAB™ showed that the calculated flutter speed of the FAST model in its baseline CG position configuration was 23.51*m/s* at a frequency of 5.98*Hz*. Similarly, the calculated flutter speed for a forward CG position configuration was 20.18*m/s* at a frequency of 6.06*Hz*. and the calculated flutter speed and flutter frequency for the aft CG position were 29.75*m/s* and 6.12*Hz*., respectively. Closed-loop simulations performed in Simulink™ showed the model to be stable after being given an initial displacement, step input and impulse input. The controller was also shown to be robust to actual nonlinearites such as actuator free-play, saturation and rate limitation.

Open-loop wind tunnel testing in the CWT showed the flutter speed and frequency of the FAST model to be 24.28*m/s* and 5.77*Hz* for the baseline CG position, which correlated well with the predicted values of 23.51*m/s* and 5.98*Hz.*, respectively. For the forward CG position configuration, open-loop flutter was encountered at a speed of 21.40*m/s* and frequency of 6.13*Hz*. These values are in good agreement with the predicted flutter speed and frequency from an eigensolution of the state-space model of the system of 20.18*m/s* and 6.06*Hz*., respectively. Open-loop testing concluded with the model in an aft CG configuration, for which flutter occurred at a speed of 30.00*m/s* and a frequency of 6.02*Hz*., again matching the predicted flutter speed of 29.75*m/s* and frequency of 6.12*Hz*. well.

Having validated the mathematical model of the FAST model used in the active flutter suppression feedback controller design, closed-loop wind tunnel testing was performed. During these tests, with the feedback controller was activated, flutter could not be induced up to the maximum operating speed of the CWT in any of the open-loop model configurations. Subsequent tests for each CG position configuration, with the control system deactivated, demonstrated that a developed flutter cycle of the model could be suppressed within less than 3*s* upon reactivation of the control system. Based on these good results, flutter boundary extension tests were conducted in the LSWT with the model in its baseline CG position. These tests were conducted to a maximum tunnel speed of 53.91*m/s* (29.63*m/s* above the critical open-loop flutter speed of the model). Up to this speed flutter was suppressed, demonstrating an increase in the flutter

boundary of 134.3% (or 2.34 times) with a controller designed for the predicted critical flutter speed (23.51*m/s*) of the model. This translates to flutter suppression at a dynamic pressure 448.9% above (or 4.69 times) that experienced by the FAST model at its critical open-loop flutter speed.

6. Conclusions

Based on the good open- and closed-loop wind tunnel results obtained from the FAST wind tunnel model, it has been demonstrated that active flutter suppression is both a feasible and attractive means of increasing the flutter boundary of an aircraft. Because of its gentle and well defined flutter characteristics, the FAST model can be easily and safely used as both a flutter suppression demonstrator and testbed for various active flutter control algorithms.

7. Acknowledgements

The Aeronautic Systems Competency (ASC) of the Council for Scientific and Industrial Research (CSIR) is thanked for their generous and continued funding of this work. Mr Andrew Sutherland is also thanked for his help and interest throughout this research.

8. References

[1] A Small Scale Pitch-Plunge Flutter Model for Active Flutter Control Research, International Council of the Aeronautical Sciences, Anchorage, Alaska, September 2008.

[2] Fung, Y.C., 1955. *An introduction to the theory of aeroelasticity*. John Wiley and Sons, Inc., New York.

[3] Scanlan, R.H. and Rosenbaum, R. 1968. *Introduction to the study of aircraft vibration and flutter*. Dover Publications, Inc. New York.

[4] Theodorsen, T. 1949. General theory of aerodynamic instability and the mechanism of flutter, NACA-TR-496. National Advisory Commission for Aeronautics.

[5] Rodden, W.P. and Stahl, B. 1969. A strip method for prediction of damping in subsonic wind tunnel and flight flutter tests. *Journal of Aircraft*. Vol. 6, No. 1. pp. 9 - 17.

[6] Franklin, G.F *et al*. 1991. *Feedback control of dynamic systems*. Addison-Wesley Publishing Company.

[7] Farmer, M.G. 1982. A two-degree of freedom mount system with low damping for testing rigid wings at different angles of attack, NASA-TM-83302. Langley Research Center.

[8] O'Neil, T and Strganac, T.W. 1998. Aeroelastic response of an airfoil supported by nonlinear springs. *Journal of Aircraft*. Vol. 35, No. 4. pp. 616 - 622.

Copyright Statement

Appendix A: State-Space Matrices

The state-space matrices given in §2.2 are listed below for convenience. The system matrix of the binary flutter system is:

$$\mathbf{A}=\left[\begin{array}{c|c|c} -\bar{\mathbf{M}}^{-1}\bar{\mathbf{C}} & -\bar{\mathbf{M}}^{-1}\bar{\mathbf{K}} & -\bar{\mathbf{M}}^{-1}\mathcal{L}_{\delta} \\ \hline \mathbf{I}_{3\times 3} & \mathbf{0}_{3\times 3} & \mathbf{0}_{3\times 2} \\ \hline -\mathbf{Q}_1\bar{\mathbf{M}}^{-1}\bar{\mathbf{C}}+\mathbf{Q}_2 & -\mathbf{Q}_1\bar{\mathbf{M}}^{-1}\bar{\mathbf{K}} & \mathbf{Q}_1\bar{\mathbf{M}}^{-1}\mathcal{L}_{\delta}+\mathcal{L}_{\lambda} \\ -\mathbf{Q}_1\bar{\mathbf{M}}^{-1}\bar{\mathbf{C}}+\mathbf{Q}_2 & -\mathbf{Q}_1\bar{\mathbf{M}}^{-1}\bar{\mathbf{K}} & \mathbf{Q}_1\bar{\mathbf{M}}^{-1}\mathcal{L}_{\delta} \end{array}\right] \quad \text{(A1)}$$

and the input matrix is:

$$\mathbf{B}=\begin{bmatrix}\bar{\mathbf{M}}^{-1}K_{\beta} \\ \mathbf{0}_{5\times 1}\end{bmatrix} \quad \text{(A2)}$$

The measurement matrix is:

$$\mathbf{C}=\begin{bmatrix}0&0&0&1&0&0&0&0\\0&0&0&0&1&0&0&0\\0&0&0&0&0&1&0&0\end{bmatrix} \quad \text{(A3)}$$

The mass, damping and stiffness matrices given in Equation (A1) are:

$$\left.\begin{aligned}\bar{\mathbf{M}}&=\mathbf{M}_s-\mathbf{M}_a\\ \bar{\mathbf{C}}&=\mathbf{C}_s-\mathbf{C}_a\\ \bar{\mathbf{K}}&=\mathbf{K}_s-\mathbf{K}_a\end{aligned}\right\} \quad \text{(A5)}$$

where the structural matrices in Equation (A5) are:

$$\mathbf{M}_s=\begin{bmatrix} m & mx_{\alpha}b & mx_{\beta}b \\ mx_{\alpha}b & I_{\alpha} & (c-a)b^2mx_{\beta}+I_{\beta} \\ mx_{\beta}b & (c-a)b^2mx_{\beta}+I_{\beta} & I_{\beta}\end{bmatrix} \quad \text{(A6)}$$

$$\mathbf{C}_s=\begin{bmatrix}C_h&0&0\\0&C_{\alpha}&0\\0&0&C_{\beta}\end{bmatrix} \quad \text{(A7)}$$

$$\mathbf{K}_s=\begin{bmatrix}K_h&0&0\\0&K_{\alpha}&0\\0&0&K_{\beta}\end{bmatrix} \quad \text{(A8)}$$

and the "aerodynamic" matrices in Equation (A5) are[1]:

$$\mathbf{M}_a=\rho b^3\begin{bmatrix} -\frac{\pi}{b} & \pi a & T_1 \\ \pi a & -\pi b\left(\frac{1}{8}+a^2\right) & b\left[T_7+(c-a)T_1\right] \\ T_1 & -2bT_{13} & \frac{1}{\pi}bT_3\end{bmatrix} \quad \text{(A9)}$$

[1] It is shown in [4] that $T_{13}=-\frac{1}{2}\left[T_7+(c-a)T_1\right]$, thus the aerodynamic mass matrix is symmetric as required.

$$\mathbf{C}_a = \rho b^2 U \begin{bmatrix} -\frac{2\pi}{b} & -2\pi(1-a) & T_4 - T_{11} \\ 2\pi\left(\frac{1}{2}+a\right) & 2\pi ba\left(\frac{1}{2}-a\right) & b\left[T_8 - T_1 + (c-a)T_4 + aT_{11}\right] \\ -T_{12} & b\left[2T_9 + T_1 + (T_4 - T_{12})\left(\frac{1}{2}-a\right)\right] & \frac{1}{2\pi} bT_{11}(T_4 - T_{12}) \end{bmatrix} \quad \text{(A10)}$$

$$\mathbf{K}_a = \rho b^2 U^2 \begin{bmatrix} 0 & -\frac{2\pi}{b} & -\frac{2T_{10}}{b} \\ 0 & 2\pi\left(\frac{1}{2}+a\right) & 2aT_{10} - T_4 \\ 0 & -T_{12} & -\frac{1}{\pi}\left[T_5 - T_{10}(T_4 - T_{12})\right] \end{bmatrix} \quad \text{(A11)}$$

The matrices in Equation (A1) that account for aerodynamic lag are:

$$\mathbf{Q}_1 = \begin{bmatrix} 1 & b\left(\frac{1}{2}-a\right) & \frac{1}{2\pi} bT_{11} \end{bmatrix} \quad \text{(A12)}$$

$$\mathbf{Q}_2 = \begin{bmatrix} 0 & U & \frac{1}{\pi} T_{10} \end{bmatrix} \quad \text{(A13)}$$

$$\mathcal{L}_\delta = \rho b^2 U \begin{bmatrix} \frac{2\pi\delta_1}{b} & \frac{2\pi\delta_2}{b} \\ -2\pi\left(\frac{1}{2}+a\right)\delta_1 & -2\pi\left(\frac{1}{2}+a\right)\delta_2 \\ T_{12}\delta_1 & T_{12}\delta_2 \end{bmatrix} \quad \text{(A14)}$$

$$\mathcal{L}_\lambda = \begin{bmatrix} -\frac{\lambda_1 U}{b} & 0 \\ 0 & -\frac{\lambda_2 U}{b} \end{bmatrix} \quad \text{(A15)}$$